Hydration of Nebular Minerals through the Implantation-Diffusion Process

Ziliang Jin^{1,2} and Maitrayee Bose¹

¹ School of Earth and Space Exploration, Arizona State University, Tempe, AZ 85287, USA; ziliang.jin@asu.edu
² State Key Laboratory of Lunar and Planetary Sciences, Macau University of Science and Technology, Taipa, Macau, People's Republic of China Received 2020 October 26; revised 2021 April 13; accepted 2021 April 13; published 2021 June 2

Abstract

Recent studies have detected structurally bound water in the refractory silicate minerals present in ordinary and enstatite chondrite meteorites. The mechanism for the incorporation of the hydrogen is not well defined. In this paper we quantitatively examine a two-fold process involving the implantation and diffusion of nebular hydrogen ions that is responsible for the hydration of the chondritic minerals. Our simulations show that depending on critical parameters, including the flux of the protons in nebular plasma, retention coefficient, temperature of the silicate minerals, and desorption rate of implanted hydrogen, the implantation of low-energy hydrogen ions can result in equivalent water contents of \sim 0.1 wt% in chondritic silicates within 10 years. Thus, this novel mechanism operating in the nebula at 10^{-3} bar pressure and <650 K temperatures can efficiently hydrate the free-floating chondritic minerals prior to the rapid formation of planetesimals inside the snow line, and agree well with the wet accretion scenario for the inner solar system objects.

Unified Astronomy Thesaurus concepts: Solar system planets (1260); Chondrules (229); Silicate grains (1456)

1. Introduction

The quest to understand the origin of water in the inner solar system bodies has been ongoing for several decades. Recently, the hydrogen isotopic compositions measured in minerals from Itokawa regolith and ordinary chondrites provided evidence that nominally anhydrous minerals (NAMs), i.e., pyroxene, from undifferentiated inner solar system bodies contain abundant structurally bound water (200–1000 ppm by weight; Jin & Bose 2019, 2020). A wide range (80–2000 ppm) of water content in bulk ordinary chondrites has also been reported, after correcting for terrestrial contamination (Vacher et al. 2020). Chondrule mesostases in enstatite chondrites exhibit high water contents (2700-12,300 ppm; Piani et al. 2020). The detected water represented by the hydrogen in the O-H defects in the crystal structure of silicate minerals agrees with the "wet" accretion scenario for the inner solar system objects (Drake 2005). However, the mechanism responsible for the incorporation of hydrogen into these silicate minerals is not well understood.

In previous studies, several mechanisms have been proposed to explain the incorporation of hydrogen into the silicate minerals. The first mechanism is the formation of O–H bonds in the silicate minerals by directly dissolving hydrous species (H₂, H₂O, and OH) into the melts, resulting in the substitution of hydrogen for other species (e.g., Mg or Al; Hauri et al. 2006). This process has been regarded as the gas-melt interaction and is dependent on several important parameters, such as the oxygen fugacity and the pressure of the melts. It has been shown that nitrogen has a high solubility in reduced basaltic melts, where oxygen fugacity is lower than the ironwüstite buffer (IW; e.g., Libourel et al. 2003; Boulliung et al. 2020). However the solubility of hydrogen in silicate melts is weakly dependent on the oxygen fugacity (e.g., Kadik et al. 2015). More importantly, relative to oxygen fugacity, the pressure of the melt seems to be a more critical parameter (e.g., Hirschmann et al. 2012). Petrological experiments on terrestrial samples revealed that high pressures (on the order of tens of gigapascal) are required for the incorporation of a large amount of hydrogen (e.g., Mierdel et al. 2007; Ferot & Bolfan-Casanova 2012). The NAMs from the undifferentiated small bodies are likely derived via an igneous process including melting of their precursors and recrystallizing in the nebular environment, characterized by extremely low pressure (<10⁻ GPa; Galy et al. 2000). At such low nebular pressures, <2 ppm H can be dissolved in the melts at oxygen fugacities close to the IW buffer (IW-2 to IW; Hirschmann et al. 2012). Furthermore, according to the shock wave model that is most likely responsible for chondrule formation, high temperatures of the precursor melts lasted for only 10 s of seconds to several minutes (Connolly & Love 1998), thus the gas-melt interaction ought to be limited. Overall, gas-melt interaction is not an efficient mechanism responsible for the high hydrogen contents in chondrule minerals, a different process for the incorporation of hydrogen into chondritic minerals is necessary.

An alternate mechanism, chemi-adsorption, where the water molecules from the solar nebular gas get adsorbed on the surface of silicate minerals, can lead to subsurface hydroxylation prior to their accretion into planetesimals (Muralidharan et al. 2008). However, the efficiency of this process, although unexplored for most silicate mineral compositions, has to be low, because adsorption preferably occurs at specific planes of silicates, e.g., {100} for olivine. Besides, the presence of abundant hydrogen gas in the solar nebula would decrease the coverage of water molecules on the silicate surface. Additionally, the adsorption mechanism could only result in the surface enrichment of water components under low temperatures, unlike conditions existing in the inner solar system. Thus, this mechanism is not responsible for the high water content in silicate minerals.

A third mechanism that has been invoked is hydrogen implantation during an irradiation process leading to the formation of the hydroxyl radicals in the interstellar medium (Bradley 1994; Djouadi et al. 2011). However, the efficiency of this mechanism during the first 4 Ma of our solar system history is unknown and is explored in this study. We present a model that systematically quantifies the implantation of protons, and subsequent desorption and diffusion of hydrogen

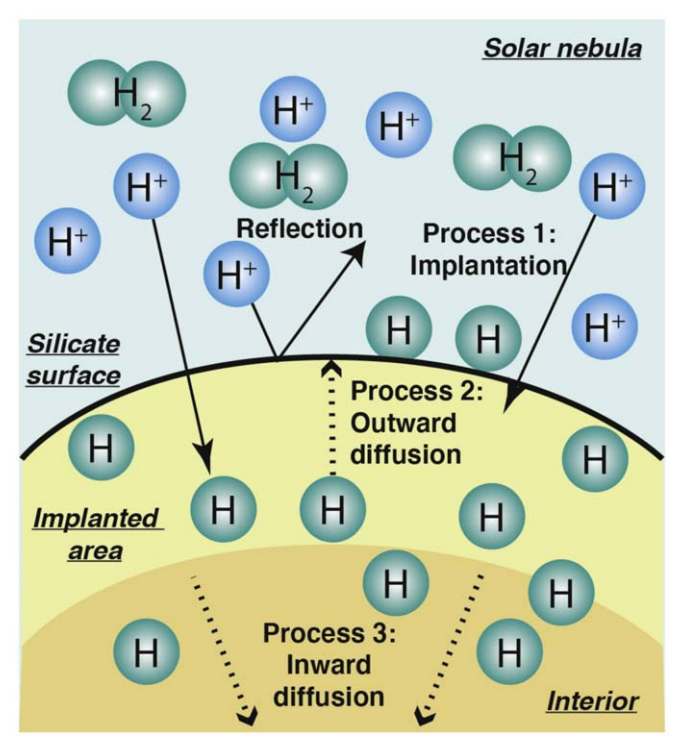


Figure 1. A schematic showing the proton implantation—diffusion processes. Ionized H^+ ions in the solar nebular gas are implanted into the top area ($\leqslant 100 \, \mathrm{nm}$) of the target silicate grain (Process 1). A fraction of the ionized hydrogen is never implanted but is backscattered to the nebular gas. Due to a concentration gradient in the implanted area of the silicate grain, a portion of the hydrogen recombines with other hydrogen atoms, diffuses outward, and desorbs from the surface of the target (Process 2). The inward diffusion of the rest of the projectile hydrogen leads to a homogeneous distribution of hydrogen in the silicate grain (Process 3).

into the silicate minerals. By simulating these processes and evaluating the key parameters affecting these processes, we explore how fast hydrogen can be incorporated in the early formed silicates prior to their accretion and how much water that corresponds to. The results of the model imply a quick accretion of small bodies in our solar system.

2. Implantation-Diffusion Model

2.1. Model Overview

Figure 1 depicts the implantation-diffusion model that includes three processes experienced by the protons in the nebular plasma, namely, implantation (Process 1), outward diffusion (Process 2), and inward diffusion (Process 3). In Process 1 abundant protons in the ionized protosolar nebula are implanted into the early condensed silicate minerals. The implantation of the nebular plasma protons is first concentrated in the surface area of the floating silicate minerals. A fraction of the implanted hydrogen subsequently diffuses outward and desorbs from the grain surface as hydrogen molecules (Process 2). The remaining fraction of the implanted hydrogen diffuses inward and distributes homogeneously in the interior of the silicate minerals (Process 3). In this model, we define the uppermost interface of the silicate exposed in the solar nebular gas as the surface, the area under the surface where H⁺ gets implanted as the implanted area (≤100 nm thick), and the remaining silicate grain as the interior.

2.2. Process 1: Implantation

Three types of protons with various origins, i.e., the protons from the ionized solar nebular gas, the solar wind (SW), and the galactic cosmic rays (GCRs), can be potentially implanted into solid materials. The unidirectional flux of protons in the observed SW ($F_{\rm SW}$) and GCRs ($F_{\rm GCR}$) are (2–3.8) × 10⁸ cm⁻² s⁻¹ and ~4 cm⁻² s⁻¹, respectively (Diodato et al. 1974; Gosling 2014; Prettyman 2014). We estimated the flux of the protons in random flow directions in the nebular plasma ($F_{\rm NP}$) via the equation

$$F_{\rm NP} = f_{\rm ion} \, v_{\rm g} \, \rho_{\rm H},\tag{1}$$

where $f_{\rm ion}$ is the ionization fraction of nebular plasma hydrogen, v_g (cm⁻² s⁻¹) is the gas–grain velocity, and $\rho_{\rm H}$ (cm⁻³) denotes the atomic density of H atoms, which can be approximated by the empirical relationship (Consolmagno & Jokipii 1978)

$$\rho_{\rm H} = 1.45 \times 10^{22} \frac{P}{T},\tag{2}$$

where P (bar) is the solar nebular pressure in the chondrule-forming region and T(K) is the ambient nebular temperature in that region.

Because the projectile $\mathrm{H^+}$ ions have the lightest mass, they can either enter the crystal lattice of the target silicate or undergo elastic collisions with atoms of the target and eventually be reflected (Amano & Seidman 1981). The retention coefficient (N_R) is employed to denote the fraction of the ions that are implanted in the target. Accordingly, the effective flux (F_{eff}) that is implanted is indicated by

$$F_{\text{eff}} = (F_{\text{NP}} + F_{\text{SW}} + F_{\text{GCR}})N_R. \tag{3}$$

2.3. Process 2: Outward Diffusion

The implantation of the protons is coupled with the diffusion processes, namely, the outward and inward diffusion within the silicate grain. Once the H⁺ ions are implanted in the top surface layer of the silicate, they will react with other atoms and will be physically trapped in the lattice defects. The concentration gradient of hydrogen within the implanted area then leads to the outward release of the implanted hydrogen. On the silicate surface, the released H atom can recombine with other H atoms, form H₂ molecules, and desorb from the surface via the reactions \equiv Si-OH $\rightleftharpoons \equiv$ Si-O + H⁰ and 2H⁰ \rightarrow H₂ (Griscom 1984), where H⁰ denotes the atomic H. The flux of the outward diffusion (F_{out}) of the implanted H⁺ after a certain time (t) is approximated by

$$F_{\rm out}(t) \approx D_{\rm im} \frac{C_{\rm im}(t) - C_{\rm out}}{h},$$
 (4)

where h is the thickness of the implanted area, which is assumed as 10^{-5} cm based on SRIM simulations (Ziegler et al. 2010). $D_{\rm im}$ is the average diffusivity of the implanted H in minerals and can be obtained by

$$D_{\rm im} = D_0 \exp\left(\frac{-\Delta H}{R_g T}\right),\tag{5}$$

where D_0 (cm² s⁻¹) is the diffusive coefficient for H in minerals and ΔH (J mol⁻¹) is the activation enthalpy. R_g is the gas constant (8.314 J mol⁻¹ K⁻¹). In Equation (4), $C_{im}(t)$ is the

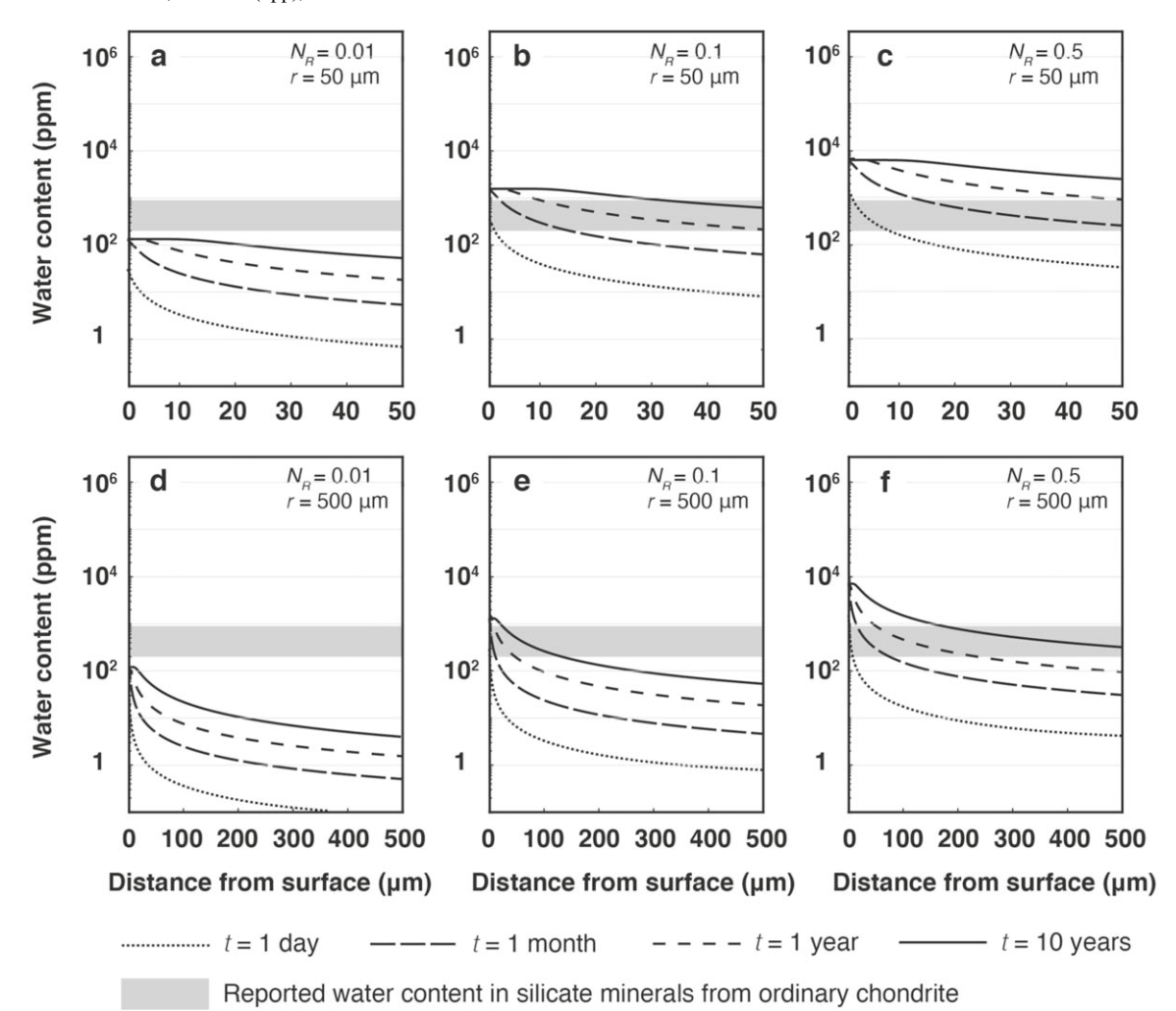


Figure 2. Simulated concentration profiles of water in the interior of the silicates. Spherical silicates with radii of $50 \ \mu m$ (a)–(c) and $500 \ \mu m$ (d)–(f) are assumed to be implanted with nebular plasma hydrogen for 1 day, 1 month (30 days), 1 year (365 days), and 10 years (3650 days). Three retention coefficients (N_R), i.e., 0.01, 0.1, and 0.5, are applied for the implantation. With the same retention coefficient (e.g., $N_R = 0.01$), it takes a longer time for $500 \ \mu m$ sized silicate (d) to evenly distribute the projectile ions than the $50 \ \mu m$ sized silicate (a). The higher retention coefficient leads to the larger production of water. For instance, implantation with a retention coefficient of 0.5 can produce more than 1000 ppm water in one year in the $50 \ \mu m$ sized silicate (c), whereas when the retention coefficient is 0.01, the production is less than 200 ppm (b). The gray shaded area indicates the range of previously reported water contents (200–1000 ppm) of the ordinary chondritic minerals, which can be well produced by the implantation–diffusion processes with $N_R > 0.1$ ((b), (c), (e), (f)). Boundary conditions for the simulations are listed in Table 1.

average atomic concentration of the projectile H^+ in the implanted area after the accumulated implantation within a duration of t and can be obtained by

$$C_{\rm im}(t) = \sum_{1}^{t} \frac{(F_{\rm eff} - F_{\rm out}(t-1))St}{V_{\rm im}},$$
 (6)

where S (cm²) is the surface area of target silicate and $V_{\rm im}$ (cm³) is the volume of the implanted area. $C_{\rm out}$ is the atomic concentration of the free H atoms in the outside reservoir, right above the surface of the silicate, which can be obtained by

$$C_{\text{out}} = \rho_{\text{H}} N_{\text{S}},\tag{7}$$

where N_S is the sticking coefficient of hydrogen atoms on the surface of one specific material.

2.4. Process 3: Inward Diffusion

By contrast, inward diffusion plays an important role to evenly distribute the implanted H and hydrate the interior of the silicate grain. The converted concentration profile of water (ppm) present between the deeper interior and the H-implanted area near the surface is simulated based on the corresponding solution to Fick's second law for spherical geometry (Ingrin & Blanchard 2006):

$$C(t, r) = \frac{M_{\text{mol}} C_{\text{im}}(t)}{N_{\text{A}} \rho_{s} V_{\text{im}}} \left(1 - \frac{6}{\pi^{2}} \sum_{n=1}^{\infty} \frac{1}{n^{2}} \exp\left(\frac{-D_{\text{im}} n^{2} \pi^{2} t}{r^{2}} \right) \right),$$
(8)

where $M_{\rm mol}$ is the molar mass of water ($M_{\rm mol} = 18 \text{ g mol}^{-1}$); $N_{\rm A}$ is Avogadro's constant ($6.02 \times 10^{23} \text{ mol}^{-1}$); ρ_s is the density of the implanted silicate, which is assumed as that of pyroxene (3.52 g cm^{-3}); and r is the distance from one specific location in the silicate's interior to its surface.

3. Results

3.1. Boundary Conditions

In the standard case, we assumed spherical orthopyroxene minerals with radii of $50 \mu m$ (Figures 2(a)–(c)) and $500 \mu m$

Table 1Boundary Conditions Applied for the Standard Case

Parameter	Symbol	Adopted Value	Unit	Reference
Gas-grain velocity	v_g	10^{6}	cm s ⁻¹	(1)
Nebular temperature in the chondrule-forming region	\overline{T}	650	K	(2)
Ionization fraction of the nebular hydrogen	$f_{ m ion}$	10^{-11}		(3), (4)
Diffusion coefficient	D_0	1.8×10^{-4}	$\mathrm{cm}^2~\mathrm{s}^{-1}$	(5)
Activation energy for hydrogen diffusion	ΔH	213	$kJ mol^{-1}$	(5)
Sticking coefficient	N_s	10^{-9}		(6)

References. (1) Wu & Judge (1979), (2) Lewis (1972), (3) Fromang et al. (2002), (4) Öberg et al. (2011), (5) Stalder & Skogby (2003), (6) Dürr & Höfer (2006).

(Figures 2(d)–(f)) condense in a region with a heliocentric distance of 1 au from the proto-Sun. The minerals are implanted by the protons in the solar nebula for 1 day, 1 month (30 days), 1 year (365 days), and 10 years (3650 days). For both silicates, the simulations were run with retention coefficients (N_R) of 0.01, 0.1, and 0.5. Other critical boundary conditions applied for our standard case are listed in Table 1.

We first adopt a high nebular gas pressure ($P=10^{-3}$ bar) for the chondrule formation (Galy et al. 2000). The ambient temperature when chondrule minerals formed was characterized by a range of temperatures, from <600 K to >900 K (Rubin 2000). The presence of a primary trolite in type 3 ordinary chondrites indicates an ambient nebular temperature of <650 K (Rubin et al. 1999). Accordingly, we select this value as the background temperature for the implantation and diffusion. In previous studies, the ionization fraction ($f_{\rm ion}$) of protoplanetary disks have been reported to be with orders between 10^{-12} and 10^{-10} (Fromang et al. 2002; Öberg et al. 2011) and we adopt a median value of 10^{-11} .

Due to the lack of the parameters applicable to the low-temperature (650 \pm 100 K) diffusion of hydrogen in nominally anhydrous silicate minerals, here we use the diffusion coefficient (D_0) and activation energy (ΔH) obtained from the experiments conducted on orthopyroxene in a temperature range of 973–1173 K (Stalder & Skogby 2003).

3.2. Standard Case

The profiles of water concentration in the orthopyroxene minerals, computed by the simulations, are indicated in Figure 2. Overall, larger-sized minerals require a longer duration of implantation and diffusion to get homogeneously distributed water profiles. For instance, with a retention coefficient of 0.01, in 10 years the implanted hydrogen could be almost homogeneously distributed in the 50 μ m sized grain (Figure 2(a)), whereas the core of the 500 μ m sized grain has much less water than the area close to the surface (Figure 2(d)). On the other hand, the retention coefficient of the projectile ions can significantly affect the water-incorporation process. With low retention coefficients (e.g., $N_R = 0.01$), the addition of water is less than 200 ppm for both the 50 μ m (Figure 2(a)) and 500 μ m (Figure 2(d)) silicates in 10 years. In contrast, high- N_R implantation (e.g., $N_R = 0.5$) can produce up to 1000 s ppm water (Figures 2(c) and (f)).

4. Discussion

The critical parameters dominating the amount of implanted hydrogen include the total flux of the protons ($F_{\rm NP}+F_{\rm SW}+F_{\rm GCR}$), the energy of the protons, the retention coefficient (N_R), the desorption rate of the implanted hydrogen ($F_{\rm out}$), the

temperature of the silicate minerals, and the duration of the implantation—diffusion process (*t*). Below we discuss how each of these affect the results.

4.1. Total Flux of Protons in the Nebula Plasma

Among the protons from various sources in the solar nebula, the GCR protons are characterized by the smallest flux ($F_{\rm GCR} = \sim 4 \, {\rm cm}^{-2} \, {\rm s}^{-1}$; Prettyman 2014). As a result, in 10 Ma, <1 ppm water can be made via implantation of GCR protons in a 50 μ m sized silicate mineral, assuming a N_R value of 1. This amount of water is negligible relative to that produced by the SW protons and the ionized nebular gas.

The implantation of SW protons has been proposed as the source of the hydroxyl components detected in the regolith grains in airless bodies, e.g., the Moon (Starukhina 2006; Tucker et al. 2019). Our calculation shows that the flux of hydrogen particles from the nebular plasma ($F_{\rm NP}$) is up to \sim 3 orders of magnitude higher than the flux of the SW protons ($F_{\rm SW}$). Hence, in a gaseous, plasma environment, the protons from the ionized solar nebula gas are the major components of the total implanted particles.

As indicated by Equations (1) and (2), the flux of the protons from the nebular plasma is a function of the temperature (T), pressure (P), and ionization fraction ($f_{\rm ion}$) of the solar nebula. Lewis (1972) assumed an adiabatic relationship between T and P in the nebula, which rationalized the mean mass densities of the planets that formed at different radial distances. Using this model, we estimated the total flux of the nebular plasma protons as a function of the heliocentric distances and plotted them in Figure 3. The profiles show that in the chondrule formation region (1–3 au; Morris et al. 2012; Desch et al. 2018), the total flux of the nebular protons can be up to a value in an order of 10^{12} cm⁻² s⁻¹, which corresponds to the water content at a level of the weight percent based on our standard case.

4.2. Energy of the Implanted Protons

Early evolution of low-mass stars $(0.2-2\ M_{\odot})$ is characterized by active emission of X-rays (Feigelson & Montmerle 1999). The emitted X-ray photons can penetrate and ionize the nebular gas in the protosolar disk (Igea & Glassgold 1999). The energy spectrum of the ionized hydrogen in the nebular plasma is unknown. However, observations of young stellar objects show that the X-rays are characterized by photons accelerated to $0.5-10\ \text{keV}$ (Stäuber et al. 2005). We thus speculate that the ionized hydrogen particles with energies of a few kiloelectronvolts were dominant in the nebular plasma. Because these hydrogen ions from the nebular plasma are the major particles implanted into the silicate minerals, we

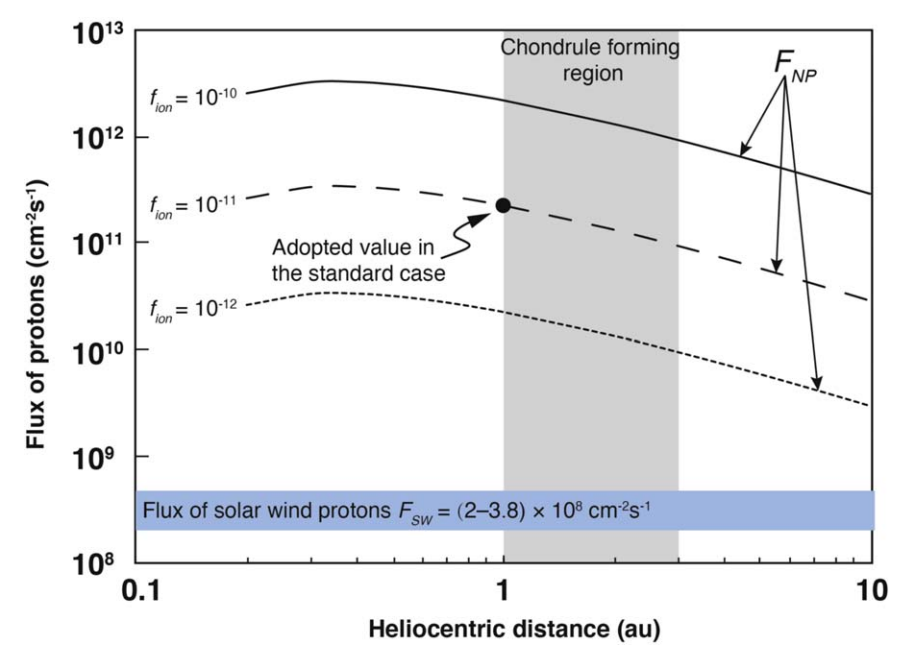


Figure 3. Flux of protons from the nebular plasma (F_{NP}) and SW (F_{SW}) as a function of the distance from the proto-Sun. The three curves indicate the F_{NP} values that were calculated with ionization fraction (f_{ion}) values of 10^{-10} , 10^{-11} , and 10^{-12} , based on Equations (1) and (2), and the proposed relationship between T and P in the nebula by Lewis (1972). For comparison, the flux of SW protons (F_{SW}) is indicated by the light blue bar, which is at least 2 orders of magnitude lower than F_{NP} . The gray area indicates the region where chondrules generally formed (1–3 au from the proto-Sun; Morris et al. 2012; Desch et al. 2018).

assumed their energies to be 10 keV in the standard case (Table 1 and Figure 2).

4.3. Retention Coefficient (N_R)

A high retention coefficient guarantees sufficient implanted ions to accumulate and diffuse inward into the interior of silicates. The hydrogen retention coefficient (N_R) in silicate minerals, e.g., olivine and pyroxene, has only been reported in a few studies. According to the ion irradiation experiments of hydrogen on amorphous SiO_2 by Schaible & Baragiola (2014), the implantation of $10 \, \text{keV}$ protons produces a higher column density of OH than that produced by 2–5 keV protons. Therefore, protons with high energy ought to be characterized by high N_R .

On the other hand, in the experiment by Lord (1968), retention coefficients of the He implantation were observed as 0.2 for enstatite, 0.2 for forsterite, and 0.4 for dunite, under the same performing conditions. Thus, N_R values of hydrogen implantation vary according to the type of minerals. In addition, the 2 keV irradiation experiment conducted on the forsterite revealed a hydrogen retention coefficient of up to 0.9 (Lord 1968). Based on these reported experimental results, we expect that the implantation of protons in the energy order of kiloelectronvolts can easily attain N_R values of >0.1, and under such a condition the production of the OH bond in silicates can reach a level of 10^3 ppm.

4.4. Desorption of Hydrogen

As indicated by Equations (4), (6), and (7), the accumulation of the implanted H ions continuously increases the concentration gradient going from the implanted area to the outmost surface as well as the flux of outward-diffused hydrogen (F_{out}). Previous studies on the lunar regolith have suggested that outward diffusion plays a significant role in reducing the retention of implanted hydrogen in the airless bodies

(Starukhina 2006). However, in our model, the target silicates implanted with H ions are immersed in abundant H_2 gas. Under such conditions, the reaction \equiv Si–O + $H_2 \rightarrow \equiv$ Si–OH + H^0 is likely to take place. Therefore, the presence of hydrogen gas surrounding the silicate grain would suppress the recombination of hydrogen atoms.

As the implantation continues, at one time the desorption rate will increase to an equal level to the effective flux of implanted hydrogen ($F_{\rm eff} = F_{\rm out}$) and lead to the equilibrium between the implantation and desorption in a short time. On the other hand, once the equilibrium is reached, the concentration of hydrogen in the implanted area stays at a constant value (Figures 2(a)–(c)). Subsequently the implanted hydrogen ions will compensate those diffused inward to the interior. As a result, the desorption process dominates the upper limit of the water concentration that is produced in the minerals via the implantation–diffusion process.

One special circumstance is that the flux of the outward diffusion reaches its upper limit (F_{out}^*) when the implanted hydrogen ions occupy all vacancies (Starukhina 2006). The saturated outward diffusion flux (F_{out}^*) is estimated based on the Polanyi-Wigner rate equation (Petermann 1972)

$$F_{\text{out}}^* = \nu I \exp\left(\frac{-\Delta E_d}{k_B T}\right),\tag{9}$$

where ν is the frequency factor, I denotes the instantaneous coverage of H atoms on the surface, and ΔE_d is the desorption activation energy of H in minerals. k_B is the Boltzmann constant $(8.617 \times 10^{-5} \, \text{eV} \, \text{K}^{-1})$. Using the reported values of ν $(10^{12} \, \text{s}^{-1})$, I $(10^7 \, \text{cm}^{-2})$, and ΔE_d $(0.75 \, \text{eV})$ from previous literature (Biham & Lipshtat 2002; Lemaire et al. 2010; Poston et al. 2015), we calculated the saturation value of the outward flux and found it to be \sim 3 orders higher than F_{eff} . In our implantation–diffusion model, this value cannot be reached,

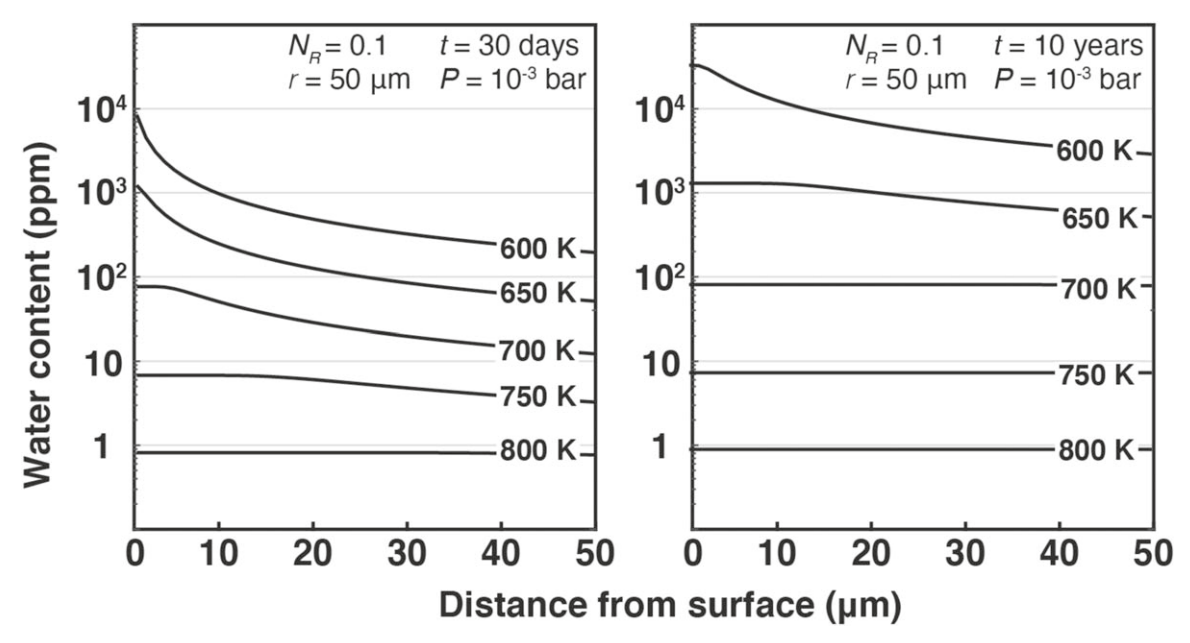


Figure 4. Concentration profiles of water in the 50 μ m sized pyroxene at temperatures of 650–800 K. Implantation was simulated in the 1 month (30 days) and 10 year (3650 days) durations and with a retention coefficient (N_R) of 0.1. The nebular pressure is set as 10^{-3} bar. The higher temperatures lead to the larger outward-diffusion rates and the smaller amounts of the remaining hydrogen ions in the silicate interior. Silicate minerals cannot receive more than 10 ppm water when the temperature is higher than 750 K.

because the $F_{\rm out}$ can only increase to a number equal to the $F_{\rm eff}$ and then the implantation remains at the equilibrium state.

4.5. Temperature of the Silicate Minerals

Generally, the silicate minerals in chondrules experience a cooling process once crystallized from their precursor melts at a peak temperature of >1800 K (Krot et al. 2001), thus how high temperatures affect the implantation process needs to be evaluated. In Figure 4, we plotted the concentration profiles of implanted water in a 50 μ m sized chondrule mineral at different temperatures (600–800 K). The results show that at an elevated temperature, chondrule minerals receive a vanishingly small amount of water via implantation, e.g., when the temperature of the silicate is higher than 800 K, the amount of water produced by implantation is less than 10 ppm in a year. Because the outward-diffusion rate of hydrogen highly depends on the temperature of the mineral, more implanted hydrogen ions would desorb from the mineral surface at a higher temperature. As a result, the net amount of hydrogen in the interior of the silicate mineral is small. However, due to the rapid cooling rate $(10-1000 \, \text{K hr}^{-1}; \, \text{Desch \& Connolly 2002}),$ cooling down of chondrule minerals to ambient temperature usually takes several hours to a few days. Besides, the temperatures of both the gas and dust in protoplanetary disks around T Tauri stars are roughly uniform (Heinzeller et al. 2011) and show a range between 350 and 700 K for distances of 0.3-1 au from the star (being considerably cooler in the midplane; Lesniak & Desch 2011). Therefore, chondrule minerals embedded in the cool solar nebula (<650 K) can receive a significant amount of water during their long residence time, despite the implantation process being inefficient for the first few hours or days after their formation.

4.6. Duration of the Implantation-Diffusion Process

Nebular gases disperse along with the evolution of the solar system in the first 3.8 million years after the formation of Ca-

Al-enriched inclusions (CAIs; Wang et al. 2017), which results in a reduced flux of the nebular protons. We then calculated the concentrations of water in a 50 μ m sized pyroxene after 30 day and 10 year of implantation at nebular pressures (P) of 10^{-5} bar, 10^{-4} bar, and 10^{-3} bar, and plotted the profiles in Figure 5. The results show that in a low-pressure nebular environment $(P = 10^{-5} \text{ bar})$, silicate minerals can only receive 10 s ppm water via implantation, which is 2 orders of magnitude lower than that produced at a pressure of 10⁻³ bar. Besides, the implantation of protons into the silicate minerals will stop when the minerals accrete to form decimeter-sized bodies and finally planetesimals. Hence, to produce a high content of water in silicate minerals floating around in the gas, the duration of the implantation-diffusion process cannot be long. Previous models suggest that planetesimals with a maximum size of \sim 100 km can form within 1 Ma (Johansen & Lambrechts 2017). Our work here suggests the incorporation of hydrogen into silicate minerals, followed by the growth of planetesimals in the inner solar system, can ideally occur in an even smaller timescale of tens of years. Accordingly, we propose that the best window of time for the hydration of silicate minerals is the first 1 Ma after their condensation at an ambient pressure of 10⁻³ bar, as suggested to occur in the chondrule-forming region. Besides, chondrules in ordinary chondrites (OCs) and carbonaceous chondrites (CCs), except Renazzo-type carbonaceous chondrites (CRs), are considered to form almost contemporaneously (2-3 Ma after the formation of CAIs) in two separated reservoirs (Pape et al. 2019). Therefore, chondrules from these classes can accumulate abundant hydrogen through ion implantation. CR chondrites are shown to be younger (2.5-4 Ma after the formation of CAIs; Desch et al. 2018; Pape et al. 2019); we predict based on our model that chondrules belonging to the CR class would contain a smaller amount of implanted hydrogen.

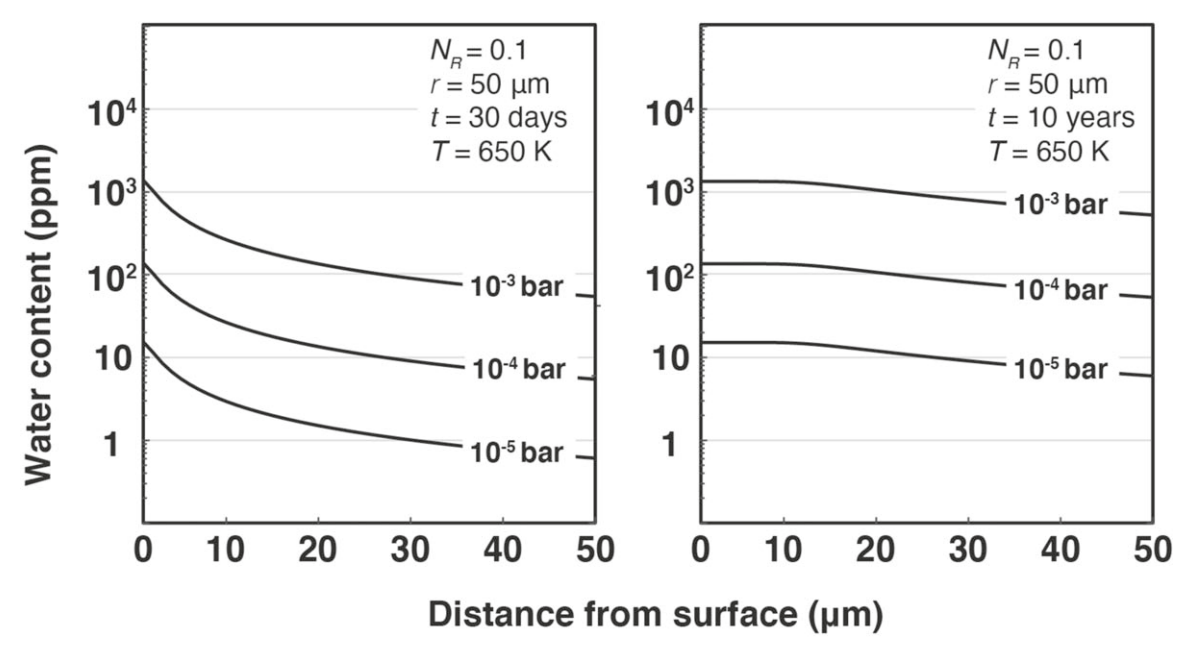


Figure 5. Concentration profiles of water in the 50 μ m sized pyroxene at various nebular pressures. Implantation was simulated at 650 K in the 1 month (30 days) and 10 year (3650 days) durations and with a retention coefficient (N_R) of 0.1. Gaseous pressure decreases along with the dissipation of nebular gases, which results in reduced fluxes of ionized hydrogen and contents of water incorporated in silicate minerals via H implantation. The formation of chondrules is expected to occur at high gas pressures (up to 10^{-3} bar) in the solar nebula (Galy et al. 2000).

4.7. Additional Considerations

The ratio between deuterium and hydrogen (D/H) has been widely employed as a tracer for the source of water in inner solar system bodies (e.g., Robert 2006). Based on our implantation-diffusion model, if hydrogen and deuterium have comparable physiochemical properties, the D/H ratio of the implanted ions in silicate minerals should be similar to that of the nebular gas, of which the best estimated D/H ratio is $\sim 0.2 \times 10^{-4}$ (Geiss & Reeves 1981). It has been shown that, however, among the reported D/H values for solid extraterrestrial samples, even the lowest number detected from the ordinary chondrite Benenitra (0.86×10^{-4}) is >4 times higher than that of nebular gas (Jin & Bose 2020). Because D/H ratios measured in bulk OCs do not drastically change with increasing degrees of thermal metamorphism (Vacher et al. 2020), the reason responsible for the high D/H ratios in chondrule minerals can be the nonidentical kinetic behaviors of hydrogen and deuterium during ionization and implantationdiffusion processes, which unfortunately has not been well studied. Hence, comprehensive laboratory experiments that determine the ionization rate, implantation efficiency, and diffusion rate of deuterium in a variety of silicate minerals are needed.

The implantation of SW ions has been considered as a significant mechanism for introducing noble gas components into meteoritic phases as well as shaping the noble gas isotopic ratios (e.g., Ott 2014; Moreira & Charnoz 2016; Péron et al. 2017). Analogously, we suspect that the solar nebular plasma contained noble gas components that were characterized by distinct properties from the SW. Implantation of the noble gas ions in the nebular plasma can be an alternative source of the noble gas components in the meteoritic phase. The evaluation of the behavior of the noble gas ions in the nebular plasma requires well-determined parameters, such as fluxes and retention coefficients of the noble gas particles; these

parameters are unknown and their discussion is beyond the scope of this work.

5. Summary

We have quantitatively evaluated the implantation and diffusion process of the nebular plasma hydrogen ions and propose that this two-fold process is responsible for the quick hydration of chondritic silicate minerals at nebular pressures of up to 10^{-3} bar, prior to the accretion of planetesimals. Apart from the individual minerals or chondrules, various objects soaked in the solar nebular plasma, such as the regolith of planetesimals and free-floating particles produced by impacts, can also be efficiently hydrogenated as a result of this implantation—diffusion process. Accordingly, the incorporated hydrogen in the silicate minerals floating in the cool gaseous nebula at <650 K could be a critical source of hydrogen/water in the objects that formed in the first 4 Ma after the formation of CAIs in our solar system.

We thank Rolf Jansen, Peter Williams, and Richard Hervig for their helpful discussions and comments to improve the original manuscript. We would also like to thank the anonymous reviewer for the constructive comments that significantly improved this manuscript. M.B. was funded by her start-up funds from Arizona State University for this work.

ORCID iDs

Ziliang Jin https://orcid.org/0000-0002-1852-9362 Maitrayee Bose https://orcid.org/0000-0002-7978-6370

References

Amano, J., & Seidman, D. N. 1981, JAP, 52, 6934 Biham, O., & Lipshtat, A. 2002, PhRvE, 66, 056103 Boulliung, J., Füri, E., Dalou, C., et al. 2020, GeCoA, 284, 120 Bradley, J. 1994, Metic, 29, 447

```
Connolly, H. C., & Love, S. G. 1998, Sci, 280, 62
Consolmagno, G. J., & Jokipii, J. R. 1978, M&P, 19, 253
Desch, S., & Connolly, H., Jr. 2002, M&PS, 37, 183
Desch, S. J., Kalyaan, A., & Alexander, C. M. 2018, ApJS, 238, 11
Diodato, L., Moreno, G., Signorini, C., & Ogilvie, K. 1974, JGR, 79, 5095
Djouadi, Z., Robert, F., d'Hendecourt, L. L. S., et al. 2011, A&A, 531, A96
Drake, M. J. 2005, M&PS, 40, 519
Dürr, M., & Höfer, U. 2006, SurSR, 61, 465
Feigelson, E. D., & Montmerle, T. 1999, ARA&A, 37, 363
Ferot, A., & Bolfan-Casanova, N. 2012, E&PSL, 349, 218
Fromang, S., Terquem, C., & Balbus, S. A. 2002, MNRAS, 329, 18
Galy, A., Young, E. D., Ash, R. D., & O'Nions, R. K. 2000, Sci, 290, 1751
Geiss, J., & Reeves, H. 1981, A&A, 93, 189
Gosling, J. T. 2014, in Encyclopedia of the Solar System, ed. T. Spohn,
   D. Breuer, & T. Johnson (Amsterdam: Elsevier), 261
Griscom, D. L. 1984, JNCS, 68, 301
Hauri, E. H., Gaetani, G. A., & Green, T. H. 2006, E&PSL, 248, 715
Heinzeller, D., Nomura, H., Walsh, C., & Millar, T. J. 2011, ApJ, 731, 115
Hirschmann, M. M., Withers, A., Ardia, P., & Foley, N. 2012, E&PSL, 345, 38
Igea, J., & Glassgold, A. 1999, ApJ, 518, 848
Ingrin, J., & Blanchard, M. 2006, RvMG, 62, 291
Jin, Z., & Bose, M. 2019, SciA, 5, eaav8106
Jin, Z., & Bose, M. 2020, LPSC, 51, 1470
Johansen, A., & Lambrechts, M. 2017, AREPS, 45, 359
Kadik, A., Koltashev, V., Kryukova, E., et al. 2015, GeocI, 53, 849
Krot, A. N., Meibom, A., Russell, S. S., et al. 2001, Sci, 291, 1776
Lemaire, J.-L., Vidali, G., Baouche, S., et al. 2010, ApJL, 725, L156
Lesniak, M., & Desch, S. 2011, ApJ, 740, 118
Lewis, J. S. 1972, E&PSL, 15, 286
Libourel, G., Marty, B., & Humbert, F. 2003, GeCoA, 67, 4123
Lord, H. 1968, JGR, 73, 5271
```

```
Mierdel, K., Keppler, H., Smyth, J. R., & Langenhorst, F. 2007, Sci, 315, 364
Moreira, M., & Charnoz, S. 2016, E&PSL, 433, 249
Morris, M. A., Boley, A. C., Desch, S. J., & Athanassiadou, T. 2012, ApJ,
  752, 27
Muralidharan, K., Deymier, P., Stimpfl, M., de Leeuw, N. H., & Drake, M. J.
  2008, Icar, 198, 400
Öberg, K. I., Qi, C., Wilner, D. J., & Andrews, S. M. 2011, ApJ, 743, 152
Ott, U. 2014, Geoch, 74, 519
Pape, J., Mezger, K., Bouvier, A.-S., & Baumgartner, L. P. 2019, GeCoA,
  244, 416
Péron, S., Moreira, M., Putlitz, B., & Kurz, M. 2017, Geochem. Perspect. Lett.,
  3, 151
Petermann, L. 1972, PrSS, 3, 1
Piani, L., Marrocchi, Y., Rigaudier, T., et al. 2020, Sci, 369, 1110
Poston, M. J., Grieves, G. A., Aleksandrov, A. B., et al. 2015, Icar, 255, 24
Prettyman, T. H. 2014, in Encyclopedia of the Solar System, ed. T. Spohn,
  D. Breuer, & T. Johnson (Amsterdam: Elsevier), 1161
Robert, F. 2006, in Meteorites and the Early Solar System II, ed.
  D. S. Lauretta & H. Y. McSween, Jr. (Tucson, AZ: Univ. Arizona
  Press), 341
Rubin, A. E. 2000, ESRv, 50, 3
Rubin, A. E., Sailer, A. L., & Wasson, J. T. 1999, GeCoA, 63, 2281
Schaible, M. J., & Baragiola, R. A. 2014, JGRE, 119, 2017
Stalder, R., & Skogby, H. 2003, PCM, 30, 12
Starukhina, L. 2006, AdSpR, 37, 50
Stäuber, P., Doty, S., Van Dishoeck, E., & Benz, A. 2005, A&A, 440, 949
Tucker, O., Farrell, W., Killen, R., & Hurley, D. 2019, JGRE, 124, 278
Vacher, L. G., Piani, L., Rigaudier, T., et al. 2020, GeCoA, 281, 53
Wang, H., Weiss, B. P., Bai, X.-N., et al. 2017, Sci, 355, 623
Wu, F., & Judge, D. 1979, ApJ, 231, 594
Ziegler, J. F., Ziegler, M. D., & Biersack, J. P. 2010, NIMPB, 268, 1818
```